Quantum tiltmeter with atom interferometry

Wen-Jie Xu, Min-Kang Zhou,* Miao-Miao Zhao, Ke Zhang, and Zhong-Kun Hu†

MOE Key Laboratory of Fundamental Physical Quantities Measurements, Hubei Key Laboratory of Gravitation and Quantum Physics, School of Physics, Huazhong University of Science and Technology, Wuhan 430074, People's Republic of China

(Received 14 June 2017; published 5 December 2017)

Matter-wave sensors with cold atoms have progressed tremendously over recent decades. We report a sensitive tilt sensor based on quantum technology employing cold atoms. This quantum tiltmeter is constructed with the configuration of a Ramsey-Bordé atom interferometer, achieving an improvement of nearly three orders of magnitude for tilt measurements with a short-term sensitivity of 1.3 μrad/Hz$^{1/2}$, with resolution down to 55 nrad at an integration time of 1000 s. The deformation of the Earth's surface has been monitored in a continuous run of 31 h, showing that a quantum tiltmeter can be applied to record tilt tides and can be an valuable sensor in geophysics and various scientific facilities.

DOI: 10.1103/PhysRevA.96.063606

I. INTRODUCTION

Atom interferometers have proven to be powerful tools in fundamental research, such as measurement of the fine-structure constant [1,2] and the Newtonian gravitational constant [3,4], as well as test of the weak equivalence principle [5–9] and the Lorentz invariance [10]. Atom interferometers are also exploited to detect gravitational waves [11–13]. Moreover, many precision sensors based on atom interferometry (AI) are developing rapidly and applied in the precision measurement of local gravity g [14–18], the gravity gradient [19–24], and rotation [25–28]. A double Bragg diffraction atom interferometer has been invented to perform tilt measurement in Ref. [29] with a sensitivity of 0.8 mrad/Hz$^{1/2}$, and potential application for tilt measurement is also possible with Raman type atom interferometers [22,25,27,28,30–32].

High precision tiltmeters are crucial sensors in scientific facilities for fundamental research. The tiltmeters are used in the advanced Laser Interferometer Gravitational Wave Observatory (advanced LIGO) to correct the tilt coupling of the inertial sensor in the seismic isolation system [33,34]. The local tilts are carefully measured and corrected in the Large Ring Laser Gyroscope [35,36] to cancel the tilt effect in the extremely sensitive and stable rotation measurement. Sensitive tiltmeters are used in absolute atom gravimeters [37,38] and atom gyroscopy [25–27] to precisely align the laser beams. Moreover, tiltmeters play unique roles in measuring the crustal deformation and are widely used in the field of volcanology [39,40], Earth tide studies [41,42], and seismology [43]. There are mainly two kinds of tiltmeters, namely long-baseline tiltmeters and short-baseline tiltmeters [44]. The long-baseline water-tube tiltmeters [45,46] with a resolution of nrad are based on the principle of communicating vessels and monitor the float positions on both sides of the instrument to measure the tilt variations. To observe the tilt variations with higher sensitivity and stability, the water-tube tiltmeters always have large dimensions of dozens of meters and were installed in some mines or caves with good thermal stability. The short-baseline tiltmeters use various forms of pendulums [44,47,48] to define the plumb line and measure the displacements between the frame and the pendulum to get the tilt variations. Thanks to the development of the microdisplacement measurement technique, the short-baseline tiltmeters can be designed compactly and portably. However, the drawback is that the short-baseline tiltmeters are sensitive to local perturbations. Recently, the laser interferometric designs [49] are used in measuring small tilt angle between two mirrors, reaching ultrahigh sensitivity.

In this paper, we report a quantum tiltmeter based on AI. The tilt signal is imprinted to the phase of atomic wave packet and measured with AI. The main features of this quantum tilt sensor are as follows: (i) The method of matter wave interferometry with well-prepared cold atoms can promise a high potential sensitivity and stability. Moreover, the employment of the atom fountain doubles the interrogation time and reduces the size of this tiltmeter, making it compact and portable for practical applications. (ii) What we measured is the tilt angle referred to the direction of freefall. The scale factor can be accurately determined, which makes the quantum type tiltmeter possible to determine the absolute direction of Earth horizontal plane. A prototype demonstration is presented below based on a symmetric Ramsey-Bordé (RB) interferometer using only one pair of Raman beams. As a precision tiltmeter, a resolution of 55 nrad is achieved at an integration time of 1000 s, and a 31-h continuous measurement shows that this quantum tiltmeter has the capability to monitor the Earth tilt tides.

II. PRINCIPLE

The principle of the experiment is sketched in Fig. 1(a). Our quantum tiltmeter is constructed by the RB atom interferometer [50] with four $\pi/2$ Raman pulses. The beam splitters of the interferometer are driven by the two-photon Raman stimulated transitions [1]. The Hamiltonian for the atom and laser field system in constant gravity can be written as [51]

$$H = H_0 + \frac{\vec{p}^2}{2M} - M\vec{g}\cdot\vec{r} + V(\vec{r},t), \tag{1}$$

where H_0 is the Hamiltonian of atomic internal states, $\vec{p}$ is the atomic momentum, M is the atomic mass, $\vec{g}$ is the local gravitational acceleration, $V(\vec{r},t)$ is the atom-laser interaction Hamiltonian, and $\vec{r}$ is the position of the atom.

*zmk@hust.edu.cn
†zkhu@hust.edu.cn

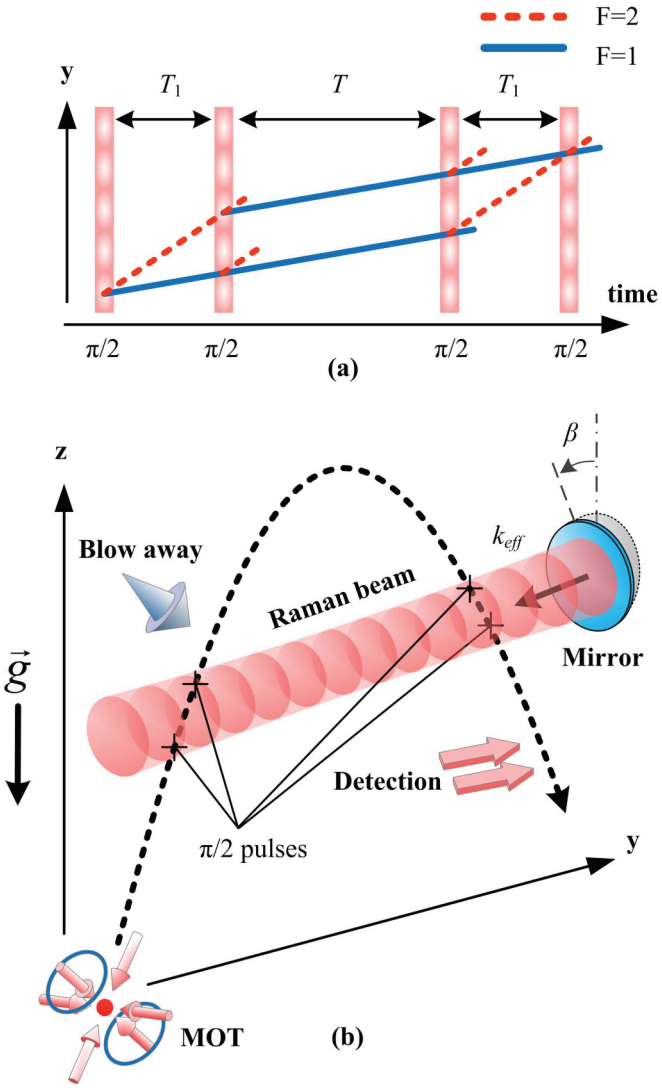

FIG. 1. (a) The space-time diagram of the RB interferometer. Only the lower interferometer is shown since the atoms in $F = 2$ are cleaned after the second Raman pulse. (b) Schematic diagram of the quantum tiltmeter based on AI. A single pair of Raman beams is used here to simplify the modulation experiment, a commercial bubble tiltmeter is fixed on the mount of the mirror (not shown in the figure) to monitor the tilt variations.

The cold atoms are illuminated successively by one pair of quasihorizontal counterpropagating Raman beams. The symmetric RB interferometer is constructed by a sequence of $\pi/2 - \pi/2 - \pi/2 - \pi/2$ pulses to coherently split, reflect, and finally combine the atomic wave packet. The total phase shift of the atom interferometer is contributed by the wave packets' free evolution ϕ_e, the final separation of the wave packets ϕ_s, and the phase due to the Raman beams ϕ_L. In an uniform gravity field, the phase shift ϕ_e and ϕ_s are calculated to be zero. During the interferometric sequence, the frequency difference between the two Raman lasers is linearly swept to compensate the projection of the Doppler shift induced by the free-falling atoms, and the ϕ_L can be expressed as:

$$\phi_L = \phi_1 - \phi_2 - \phi_3 + \phi_4, \tag{2}$$

where $\phi_i = \vec{k}_{\text{eff}} \cdot \vec{r}_i - \frac{1}{2}\alpha {t_i}^2 + \phi_0, (i = 1,2,3,4)$ is the laser phase in the current experimental setup and $\vec{k}_{\text{eff}} = \vec{k}_1 - \vec{k}_2$ is the effective wave vector of the Raman beams, α is the frequency chirp rate of the Raman beam, and $\vec{r}_i$ is the atom position at the moment of t_i when the ith Raman pulse is switched on. The first term $\vec{k}_{\text{eff}} \cdot \vec{r}_i$ is the phase induced by the local gravity, and the second term $-\frac{1}{2}\alpha {t_i}^2$ is the phase of laser due to the linearly sweeping of the frequency difference between the Raman beams. Thus, the phase shift of RB interferometer can be determined as:

$$\phi = \vec{k}_{\text{eff}} \cdot \vec{g} T_1(T_1 + T) - \alpha T_1(T_1 + T), \tag{3}$$

where T_1 is the time between the first two pulses as well as the last two pulses and T is the time between the second and third Raman pulses. We can conclude from the interferometric phase $\vec{k}_{\text{eff}} \cdot \vec{g} T_1(T_1 + T)$ that the tilt angle is extracted by measuring the projection of the gravity in the direction of Raman beams.

In our experiment, the Raman beam propagates quasihorizontally, and the angle with respect to the horizontal plane is β. The phase shift induced by the local gravity can be expanded as $k_{\text{eff}} g\beta T_1(T_1 + T) + k_{\text{eff}} g\beta^3 T_1(T_1 + T)/6 + \mathcal{O}(\beta^5)$. The high-order term $k_{\text{eff}} g\beta^3 T_1(T_1 + T)/6 + \mathcal{O}(\beta^5)$ is about 7 orders of magnitude smaller than the first-order term when $\beta < 1$ mrad, which can be neglected. Finally, the interferometric phase shift can be written as

$$\phi = \beta k_{\text{eff}} g T_1(T_1 + T) - \alpha T_1(T_1 + T). \tag{4}$$

III. OVERVIEW OF THE EXPERIMENTAL SETUP

The experimental setup is shown in Fig. 1(b). The quantum tiltmeter is based on a ultra-high vacuum chamber including three parts for the three-dimensional magneto-optical trap (3D-MOT), the matter-wave interference, and detection. About 100 million ^{87}Rb atoms are first loaded into the 3D-MOT. We then launch atoms along a parabolic trajectory using the moving molasses technique with an atomic temperature of 2.5 μK. The initial velocity of the atom cloud is about 4.27 m/s at an angle of 20.7° with respect to the vertical direction, the parabolic trajectory is used to obtain a horizontal Doppler shift for distinguishing the $\pm k_{\text{eff}}$ configurations. After a state preparation and a velocity selection, about 5×10^4 atoms with a y direction temperature of 90 nK in the state $|5\,^2S_{1/2}, F = 1, m_F = 0\rangle$ are prepared. When atoms move to the interference chamber, a Raman pulses sequence in the form of $\pi/2$- $\pi/2$- $\pi/2$- $\pi/2$ is applied to manipulate the atomic wave packet. The Raman beams are composed of two phase-locked lasers [18] with a total power of 35 mW, and the $1/e^2$ diameter is about 20 mm. The retro-reflection mirror of the Raman beams is used to realize the counterpropagating configuration, and the tilt of the mirror is monitored by a commercial bubble tiltmeter (JEWELL 775) with a resolution of 0.1 μrad. Finally, the transition probability P determined by the phase accumulated between the two arms of the interferometer is measured through a normalized fluorescence detection method. The whole time used for a single measurement is 1.1 s.

We use only one pair of counterpropagating Raman beams with one mirror to simplify the Raman system, and all four $\pi/2$ pulses are realized by the single pair of Raman beams.

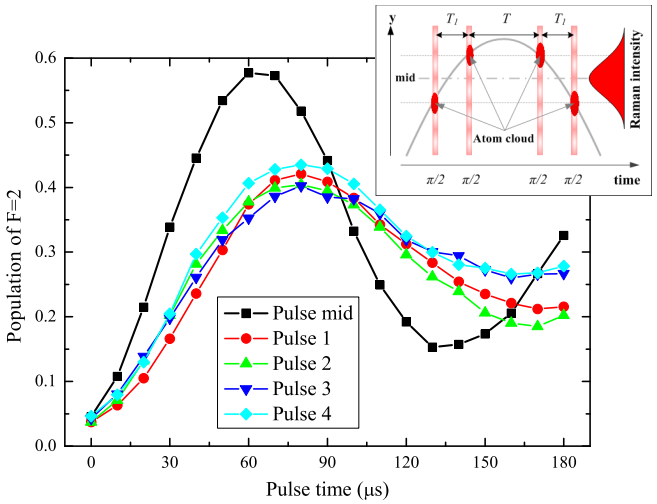

FIG. 2. Rabi oscillation at different positions. The black squares refer to the Rabi oscillation of the atom cloud located in the mid of the Raman beam, the Rabi oscillations in the position of the first $\pi/2$ pulse (the red circles), the second $\pi/2$ pulse (the green upper triangles), the third $\pi/2$ pulse (the blue lower triangles), and the fourth $\pi/2$ pulse (the cyan diamonds) are also shown in the figure when $T_1 = 8.6$ ms. The insert is the relative position of the atom cloud and the Raman beam when the ith Raman pulse is switched on.

However, the inhomogeneity of the Rabi frequency due to the Gauss distribution of the Raman beam intensity will cause a reduction of the Raman transition efficiency, which decreases the contrast of the fringe patterns. The spatial dependent contrast caused by the inhomogeneity of the Rabi frequency has been analyzed in Ref. [52] in detail. We have measured the coupling of the Raman beam when atoms locate in different positions as shown by the insert of Fig. 2. Both of the coupling and the Rabi frequency are decreased when atoms cloud locate in the edge of the Raman beam (Fig. 2). Unfortunately, we have to set the Raman transition in the edge of the Gaussian profile, because we must maximize the interrogation time of the atom interferometer to get high sensitivity. Our RB interferometer is constructed symmetrically in the experiment, $T + T_1$ is set to constant and equals 217 ms, and we set T_1 as large as possible. Finally, the contrast of the fringe patterns is just 7% during the continuous tilt measurements, which limits the total interrogation time of the quantum tiltmeter. The drop of the fringe contrast are also observed [shown in Figs. 3(a) and 3(b)] when increasing T_1.

The tilt angle β of the Raman beams is measured by changing the value of α around the central fringes [53] under different T_1; consequently, when the chirp rate compensates the projection of the Doppler shift exactly, the interference patterns locate the minimum independently of T_1, and the tilt β is determined by $\beta = \alpha/(k_{\text{eff}} g)$. The k-reversal scheme [54] is used here to eliminate some systematic effects. The fringes of the atom interferometer both in $\pm k_{\text{eff}}$ are shown in Figs. 3(a) and 3(b) with T_1 values of 4.6 ms, 6.6 ms, and 8.6 ms.

To verify the feasibility of this quantum tiltmeter, we modulate the orientation of k_{eff} by tilting the retro-reflection mirror step by step and record the tilt angles with two manners, one is from the commercial bubble tiltmeter mounted on the

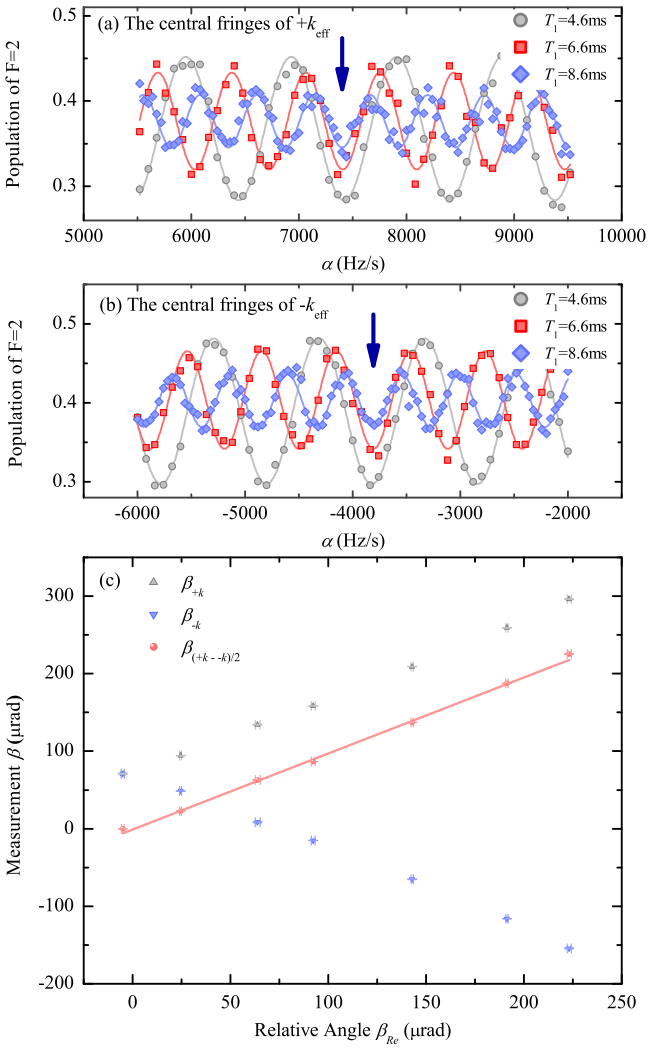

FIG. 3. [(a) and b)] Identifying the central fringe by modulate the chirp rate α with different T_1 for $\pm k_{\text{eff}}$. The data points corresponding to the gray circles, red squares, and blue diamonds are for 4.6 ms, 6.6 ms, and 8.6 ms. The royal blue arrows head to the central fringe. (c) Modulating the tilt angle of the Raman beam. The relative angle β_{Re} of the mirror is monitored by the commercial tiltmeter. The tilt in the direction of Raman beams β is measured by our quantum tiltmeter.

mirror and another one is the result of the quantum tiltmeter as described above. As shown in Fig. 3(c), we find good agreement of the tilt angles β extracted from the quantum tiltmeter and the relative tilt angles β_{Re} monitored by the commercial tiltmeter, and $\beta/\beta_{\text{Re}} = 0.98(2)$, the statistical uncertainty is most probably originated from the wave-front aberration and the temperature fluctuation during the modulation experiment. There is a bias of 70 μrad for the tilt measured by single $+k_{\text{eff}}$ or $-k_{\text{eff}}$, which is mostly caused by the light-shift due to the intensity inhomogeneity of the Raman beams. With the help of microwave [55], we adjust the light-shift nearly to zero as possible as we can to minimize the AC-Stark effect, and the k-reversal scheme is used here to eliminate the residual AC-Stark effect. Another possible contribution to the bias is the inhomogeneity of the magnetic field, which can be canceled by the k-reversal scheme as well.

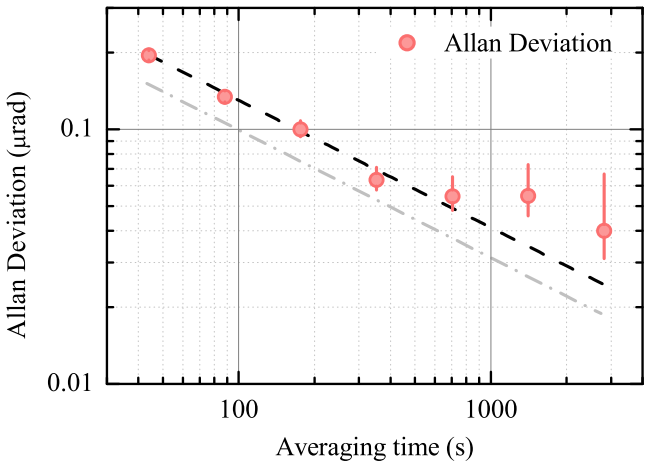

FIG. 4. Allan deviation of the quantum tiltmeter. It gives a short-term sensitivity of 1.3 μrad/Hz$^{1/2}$ for tilt measurements; the detection noise limitation (gray dash-dot line) is shown in the figure.

IV. SENSITIVITY AND NOISE TRACKING

In order to reach the maximum sensitivity of the quantum tiltmeter, we set $T_1 = 8.6$ ms during the continuous tilt measurements. The Allan deviation of the tilt measurements is shown in Fig. 4. The short-term sensitivity of the quantum tiltmeter given by the Allan deviation is 1.3 μrad/Hz$^{1/2}$, which represents an improvement of nearly three orders of magnitude for tilt measurements to previous quantum tiltmeter [29]. The stability of the tilt measurement improves as $\tau^{1/2}$ and reaches 55 nrad after an integration time of 1000 s. The long-term resolution mainly limited by the fluctuation of the temperature and the tilt tides. A short-term sensitivity of 5 μrad/Hz$^{1/2}$ has been recently reported in Ref. [56] for tilt measurements.

The detection noise usually gives limit to the sensitivity of atom interferometer [18] and should be carefully considered. The detection noise σ_P is represented by the function of the transition probability P. The transition probability is always influenced by the quantum projection noise, the electric noise, and the power or frequency noise of the detection beams [57]. The detection noise σ_P is measured by modulating the number of the atoms by the means used in Ref. [57]. Finally, the detection noise is evaluated to 1.1%, limited by the frequency noise of the detection beams. The phase noise of the quantum tiltmeter due to the detection noise and the low contrast is $2\sigma_P/Ck_{\text{eff}}gT_1(T_1+T) = 1.03$ μrad/Hz$^{1/2}$, which is close to the short-term sensitivity of 1.3 μrad/Hz$^{1/2}$ of our quantum tiltmeter.

We carefully considered the vibration noise of the reflection mirror and its effect on the sensitivity limitation of the quantum tiltmeter. The power spectrum density of the vibration noise is shown in Fig. 5(a). The effect of the vibration is evaluated by the means of the sensitivity function [58], for the symmetric RB interferometer, the sensitivity function $g(t)$ is given by

$$g(t) = \begin{cases} 0 & t < -T - T_1 \\ \sin(\Omega(T + T_1 + t)) & -T - T_1 \leqslant t < -T - T_1 + \tau \\ 1 & -T - T_1 + \tau \leqslant t < -T \\ \cos(\Omega(T + t)) & -T \leqslant t < -T + \tau \\ 0 & -T + \tau \leqslant t < T - \tau \\ -\cos(\Omega(T - t)) & T - \tau \leqslant t < T \\ -1 & T \leqslant t < T + T_1 - \tau \\ -\sin(\Omega(T + T_1 - t)) & T + T_1 - \tau \leqslant t < T + T_1 \\ 0 & T + T_1 \leqslant t \end{cases} \quad (5)$$

where Ω is the Rabi frequency and τ is the duration of the $\pi/2$ pulses. From the sensitivity function, the transfer function can be determined as

$$H_a{}^2(\omega) = \left[k_{\text{eff}}\frac{i}{2\omega}\int_{-\infty}^{\infty} g(t)d\omega\right]^2 = \frac{16k_{\text{eff}}^2\{\cos(\omega T) - \cos[\omega(T+T_1)]\}^2}{\omega^4}. \quad (6)$$

With the transfer function and the vibration noise spectroscopy shown in Fig. 5, the limitation of the vibration noise is about 0.13 μrad/Hz$^{1/2}$, which is one order of magnitude lower than the short-term sensitivity. The same method can also be used in analyzing the effect of the Raman beam phase noise and gives a sensitivity limitation of 0.03 μrad/Hz$^{1/2}$.

As a summary, the sensitivity limitations set by the main noise sources of the tiltmeter are presented in Table I.

V. EARTH TILT TIDES

An uninterrupted continuous tilt measurement for 31 h is performed to monitor the Earth tilt tides in our laboratory

TABLE I. Main noise sources to the tilt measurements.

Main noise source	Value (μrad/Hz$^{1/2}$)
Detection noise	1.03
Vibration noise	0.13
Raman laser phase noise	0.03

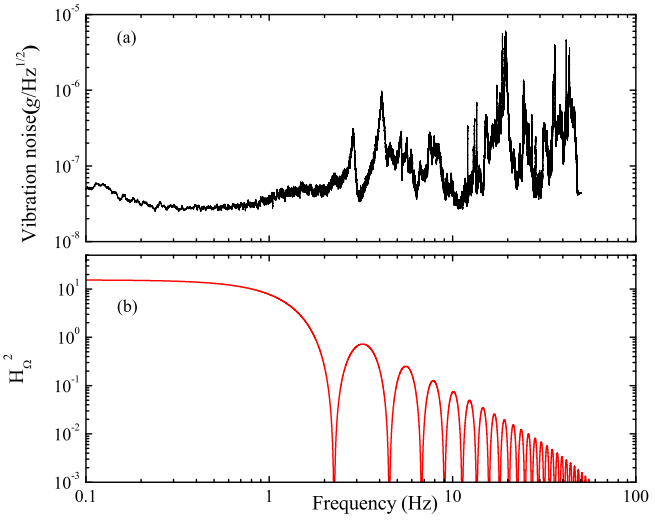

FIG. 5. The vibration noise spectroscopy (black line) and the transfer function (red line) of the symmetric RB interferometer.

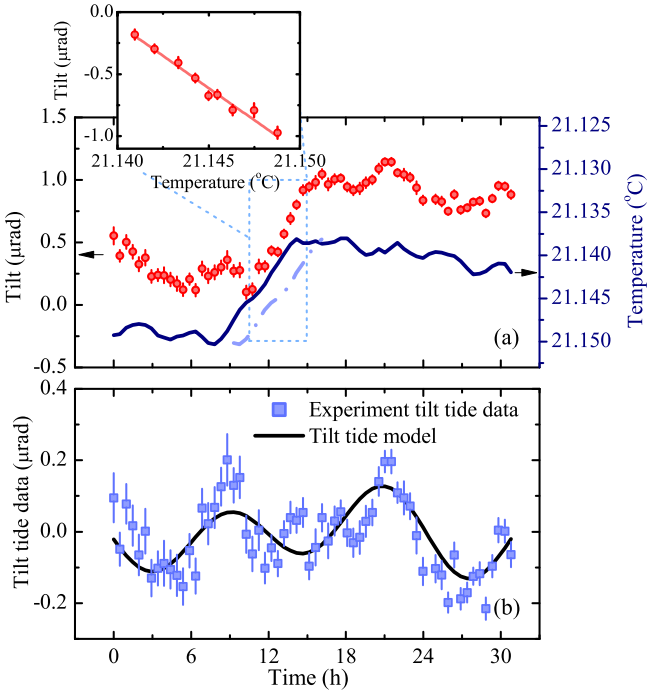

FIG. 6. A continuous tilt measurement is carried out for 31 h. (a) Red circles: Continuous tilt measurements of 31 h operated by the quantum tiltmeter between 22 and 24 January 2017. Each data point represents an average of 1760 s. The royal blue line is the monitored temperature near the reflection mirror, and the dash-dot line is the temperature shifted with a 2-h delay. The linear correlation of the tilt and temperature from 11 h to 15 h is shown in the inset. (b) The experiment tilt tide (blue squares) after temperature compensation, the black line is the theory model of the Earth tilt tide.

located in a cave. The red circles in Fig. 6(a) show the raw tilt data measured by the atom interferometer, with the room temperature [blue line in Fig. 6(a)] recorded simultaneously. Even though the fluctuation of the room temperature is extremely small, with a peak-to-peak level of 10 mK, we still see a strong correlation between the tilt and temperature. Since the components of the experiment setup have different thermal expansion coefficient, the fluctuation of the temperature and the temperature gradient introduce the deformation of experiment setup, and as a consequence, the tilt of the Raman mirror is changed. Moreover, we have observed a 2-h time delay between the temperature changes and the tilt variation, the reason of the slow response is the complex and massive experiment setup has a long thermal time constant. The correlation between the tilt and delayed temperature is shown in the insert of Fig. 6(a), which gives a coefficient of -103 nrad/mK. In addition to the temperature influence, a linear drift of -740 nrad/day is also observed, probably caused by the drift of the quartz oscillator which is used as the reference of the Raman beams' frequency chain. After being corrected from the sudden temperature change and the linear drift, the final results of the tilt measurements are shown in Fig. 6(b). Both the phase and the amplitude of the tilt measurements are consistent with the theoretical model of the Earth tilt tide, and the Pearson's correlation coefficient between the experiment and tilt tide model is 0.79, which clearly shows that this quantum tiltmeter has the capability of measuring the Earth deformation.

VI. DICUSSION

In addition to recording the tilt variation, our quantum tiltmeter can also be used to precisely measure the absolute value of the tilt angle between the $\vec{k}_{\text{eff}}$ and the horizontal plane. The tilt angle is defined by the plumb line and can be determined by $\beta = \alpha/(k_{\text{eff}} g)$. The frequency chirp rate α is determined by a high performance oscillator, and the effective wave vector $\vec{k}_{\text{eff}}$ is determined by the Raman beams' frequency, which is linked to the atomic transition line of ^{87}Rb. The frequency chirp rate α and the effective wave vector $\vec{k}_{\text{eff}}$ can be measured with high accuracy since that we can measure the frequency precisely. The absolute value of local gravity g can also be determined through an absolute gravimeter. Therefore, the tilt angle between the $\vec{k}_{\text{eff}}$ and the horizontal plane can be accurately extracted through the quantum tiltmeter. A great challenge of this absolute quantum tiltmeter is the effect of wave-front aberrations. The phase shift induced by wave-front aberrations mainly depends on the optical elements in the Raman system [59], namely the window of the vacuum chamber, the $\lambda/4$ wave plate, and the reflection mirror. The surface qualities of the $\lambda/4$ wave plate and the reflection mirror in the Raman system are about $\lambda/20$, but the surface quality of the glass window mounted to the vacuum chamber is unknown, which will induce a systematic error for the tilt measurements. As an estimate, the surface quality of the optical elements in the Raman system is about $\lambda/5$ in Ref. [59], corresponding to a systematic error of about 9 μrad in our quantum tiltmeter.

In conclusion, a quantum tiltmeter based on an RB atom interferometer has been realized with a parabolic atom fountain. The sensitivity reached by our quantum tiltmeter

allows us to monitor the deformation of Earth surface, and the quantum tiltmeter has potential important applications in geophysics. Moreover, this tiltmeter can also be integrated into quantum sensors such as atom gyroscopes and atom gravimeters to provide a more accurate calibration. Assuming a Mach-Zehnder-type interferometer with $T = 200$ ms, the quantum projection noise limitation is below 1 nrad/$\mathrm{Hz}^{1/2}$ with 10^6 atoms and a 20% contrast. The high potential sensitivity and the feature of absolute tilt measurement make the quantum tiltmeter attractive among the various tiltmeters.

ACKNOWLEDGMENT

This work is supported by the National Natural Science Foundation of China (Grants No. 91636219, No. 11474115, No. 11625417, and No. 11727809).

[1] D. S. Weiss, B. C. Young, and S. Chu, Appl. Phys. B **59**, 217 (1994).
[2] M. Cadoret, E. de Mirandes, P. Cladé, S. Guellati-Khélifa, C. Schwob, F. Nez, L. Julien, and F. Biraben, Phys. Rev. Lett. **101**, 230801 (2008).
[3] J. B. Fixler, G. T. Foster, J. M. McGuirk, and M. A. Kasevich, Science **315**, 74 (2007).
[4] G. Lamporesi, A. Bertoldi, L. Cacciapuoti, M. Prevedelli, and G. M. Tino, Phys. Rev. Lett. **100**, 050801 (2008).
[5] S. Fray, C. A. Diez, T. W. Hänsch, and M. Weitz, Phys. Rev. Lett. **93**, 240404 (2004).
[6] G. Rosi, G. D'Amico, L. Cacciapuoti, F. Sorrentino, M. Prevedelli, M. Zych, Č. Brukner, and G. M. Tino, Nat. Commun. **8**, 15529 (2017).
[7] L. Zhou, S. T. Long, B. Tang, X. Chen, F. Gao, W. C. Peng, W. T. Duan, J. Q. Zhong, Z. Y. Xiong, J. Wang, Y. Z. Zhang, and M. S. Zhan, Phys. Rev. Lett. **115**, 013004 (2015).
[8] X. C. Duan, X. B. Deng, M. K. Zhou, K. Zhang, W. J. Xu, F. Xiong, Y. Y. Xu, C. G. Shao, J. Luo, and Z. K. Hu, Phys. Rev. Lett. **117**, 023001 (2016).
[9] B. Barrett, L. Antoni-Micollier, L. Chichet, B. Battelier, T. Lévèque, A. Landragin, and P. Bouyer, Nat. Commun. **7**, 13786 (2016).
[10] H. Müller, S. W. Chiow, S. Herrmann, S. Chu, and K. Y. Chung, Phys. Rev. Lett. **100**, 031101 (2008).
[11] S. Dimopoulos, P. W. Graham, J. M. Hogan, M. A. Kasevich, and S. Rajendran, Phys. Rev. D **78**, 122002 (2008).
[12] W. Chaibi, R. Geiger, B. Canuel, A. Bertoldi, A. Landragin, and P. Bouyer, Phys. Rev. D **93**, 021101 (2016).
[13] B. Canuel, A. Bertoldi, L. Amand, E. Borgo di Pozzo, B. Fang, R. Geiger, J. Gillot, S. Henry, J. Hinderer, D. Holleville, G. Lefévre, M. Merzougui, N. Mielec, T. Monfret, S. Pelisson, M. Prevedelli, S. Reynaud, I. Riou, Y. Rogister, S. Rosat, E. Cormier, A. Landragin, W. Chaibi, S. Gaffet, and P. Bouyer, arXiv:1703.02490v2.
[14] A. Peters, K. Y. Chung, and S. Chu, Metrologia **38**, 25 (2001).
[15] J. Le Gouët, T. E. Mehlstaubler, J. Kim, S. Merlet, A. Clairon, A. Landragin, and F. Pereira Dos Santos, Appl. Phys. B **92**, 133 (2008).
[16] J. Lautier, L. Volodimer, T. Hardin, S. Merlet, M. Lours, F. Pereira Dos Santos, and A. Landragin, Appl. Phys. Lett. **105**, 144102 (2014).
[17] M. Hauth, C. Freier, V. Schkolnik, A. Senger, M. Schmidt, and A. Peters, Appl. Phys. B **113**, 49 (2013).
[18] Z. K. Hu, B. L. Sun, X. C. Duan, M. K. Zhou, L. L. Chen, S. Zhan, Q. Z. Zhang, and J. Luo, Phys. Rev. A **88**, 043610 (2013).
[19] N. Yu, J. M. Kohel, J. R. Kellogg, and L. Maleki, Appl. Phys. B **84**, 647 (2006).
[20] F. Sorrentino, Q. Bodart, L. Cacciapuoti, Y. H. Lien, M. Prevedelli, G. Rosi, L. Salvi, and G. M. Tino, Phys. Rev. A **89**, 023607 (2014).
[21] M. J. Snadden, J. M. McGuirk, P. Bouyer, K. G. Haritos, and M. A. Kasevich, Phys. Rev. Lett. **81**, 971 (1998).
[22] G. W. Biedermann, X. Wu, L. Deslauriers, S. Roy, C. Mahadeswaraswamy, and M. A. Kasevich, Phys. Rev. A **91**, 033629 (2015).
[23] X. C. Duan, M. K. Zhou, D. K. Mao, H. B. Yao, X. B. Deng, J. Luo, and Z. K. Hu, Phys. Rev. A **90**, 023617 (2014).
[24] P. Asenbaum, C. Overstreet, T. Kovachy, D. D. Brown, J. M. Hogan, and M. A. Kasevich, Phys. Rev. Lett. **118**, 183602 (2017).
[25] J. K. Stockton, K. Takase, and M. A. Kasevich, Phys. Rev. Lett. **107**, 133001 (2011).
[26] P. Berg, S. Abend, G. Tackmann, C. Schubert, E. Giese, W. P. Schleich, F. A. Narducci, W. Ertmer, and E. M. Rasel, Phys. Rev. Lett. **114**, 063002 (2015).
[27] I. Dutta, D. Savoie, B. Fang, B. Venon, C. L. Garrido Alzar, R. Geiger, and A. Landragin, Phys. Rev. Lett. **116**, 183003 (2016).
[28] A. V. Rakholia, H. J. McGuinness, and G. W. Biedermann, Phys. Rev. Appl. **2**, 054012 (2014).
[29] H. Ahlers, H. Müntinga, A. Wenzlawski, M. Krutzik, G. Tackmann, S. Abend, N. Gaaloul, E. Giese, A. Roura, R. Kuhl, C. Lämmerzahl, A. Peters, P. Windpassinger, K. Sengstock, W P. Schleich, W. Ertmer, and E. M. Rasel, Phys. Rev. Lett. **116**, 173601 (2016).
[30] R. Colella, A. W. Overhauser, and S. A. Werner, Phys. Rev. Lett. **34**, 1472 (1975).
[31] T. Lévèque, A. Gauguet, F. Michaud, F. Pereira Dos Santos, and A. Landragin, Phys. Rev. Lett. **103**, 080405 (2009).
[32] S. M. Dickerson, J. M. Hogan, A. Sugarbaker, D. M. S. Johnson, and M. A. Kasevich, Phys. Rev. Lett. **111**, 083001 (2013).
[33] F. Matichard *et al.*, Class. Quant. Grav. **32**, 185003 (2015).
[34] B. P. Abbott *et al.*, Phys. Rev. Lett. **116**, 061102 (2016).
[35] K. U. Schreiber, T. Klügel, J. P. R. Wells, R. B. Hurst, and A. Gebauer, Phys. Rev. Lett. **107**, 173904 (2011).
[36] K. U. Schreiber and J. P. R. Wells, Rev. Sci. Instrum. **84**, 041101 (2013).
[37] A. Peters, K. Y. Chung, and S. Chu, Nature (London) **400**, 849 (1999).
[38] P. Gillot, O. Francis, A. Landragin, F. Pereira Dos Santos, and S. Merlet, Metrologia **51**, L15 (2014).
[39] J. J. Dvorak and D. Dzurisin, Rev. Geophys. **35**, 343 (1997).
[40] L. N. Medina, D. F. Arcos, and M. Battaglia, J. Volcanol. Geotherm. Res. **344**, 232 (2017).

[41] P. Melchior, *The Tides of the Planet Earth* (Pergamon, Oxford, 1983).
[42] H. Ruotsalainen, Pure Appl. Geophys., doi: 10.1007/s00024-017-1562-6 (2017).
[43] Y. Ito, K. Obara, K. Shiomi, S. Sekine, and H. Hirose, Science **315**, 503 (2007).
[44] D. C. Agnew, Rev. Geophys. **24**, 579 (1986).
[45] N. D'Oreye and W. Züern, Rev. Sci. Instrum. **76**, 024501 (2005).
[46] F. Boudin, P. Bernard, L. Longuevergne, N. Florsch, C. Larmat, C. Courteille, P. A. Blum, T. Vincent, and M. Kammentaler, Rev. Sci. Instrum. **79**, 034502 (2008).
[47] Y. Cheng, J. Winterflood, L. Ju, and D. G. Blair, Class. Quant. Grav. **19**, 1723 (2002).
[48] S. Wu, S. Fan, J. Luo, and H. Hsu, Rev. Sci. Instrum. **73**, 2150 (2002).
[49] J. Martínez-Rincón, C. A. Mullarkey, G. I. Viza, W. Liu, and J. C. Howell, Opt. Lett. **42**, 2479 (2017).
[50] F. Riehle, Th. Kisters, A. Witte, J. Helmcke, and Ch. J. Bordé, Phys. Rev. Lett. **67**, 177 (1991).
[51] Ch. J. Bordé, Gen. Relativ. Gravit. **36**, 475 (2004).
[52] T. H. Kim, S. H. Yim, K. M. Shim, and S. Lee, Phys. Rev. A **95**, 033632 (2017).
[53] S. Abend, M. Gebbe, M. Gersemann, H. Ahlers, H. Müntinga, E. Giese, N. Gaaloul, C. Schubert, C. Lämmerzahl, W. Ertmer, W. P. Schleich, and E. M. Rasel, Phys. Rev. Lett. **117**, 203003 (2016).
[54] A. Louchet-Chauvet, T. Farah, Q. Bodart, A. Clairon, A. Landragin, S. Merlet, and F. Pereira Dos Santos, New J. Phys. **13**, 065025 (2011).
[55] M. K. Zhou, L. L. Chen, Q. Luo, K. Zhang, X. C. Duan, and Z. K. Hu, Phys. Rev. A **93**, 053615 (2016).
[56] X. Wu, F. Zi, J. Dudley, R. J. Bilotta, P. Canoza, and H. Müller, arXiv:1707.08693v2.
[57] A. Gauguet, B. Canuel, T. Lévèque, W. Chaibi, and A. Landragin, Phys. Rev. A **80**, 063604 (2009).
[58] P. Cheinet, B. Canuel, F. Pereira Dos Santos, A. Gauguet, F. Yver-Leduc, and A. Landragin, IEEE Trans. Instrum. Meas. **57**, 1141 (2008).
[59] M. K. Zhou, Q. Luo, L. L. Chen, X. C. Duan, and Z. K. Hu, Phys. Rev. A **93**, 043610 (2016).